CHEMISTRY OF MATERIALS
Article

Chem. Mater. **2010,** *22,* 565–578 565
DOI:10.1021/cm903368r

Structure, Electronic Structure, Optical, and Dehydrogenation Catalytic Study of $(Zn_{1-z}In_z)(O_{1-x}N_x)$ Solid Solution

Maitri Mapa,[†] Kumarsrinivasan Sivaranjani,[†] Deu S. Bhange,[†] Biswajit Saha,[‡] Purushottam Chakraborty,[‡] Annamraju Kasi Viswanath,[§] and Chinnakonda S. Gopinath*,[†]

[†]*Catalysis Division, National Chemical Laboratory, Dr. Homi Bhabha Road, Pune 411 008, India,* [‡]*Surface Physics Division, Saha Institute of Nuclear Physics, 1/AF Bidhannagar, Kolkata 700 064, India, and* [§]*Centre for Materials for Electronics Technology, Department of Information Technology, Government of India, Panchawati, Off Pashan Road, Pune 411 008, India*

Received November 4, 2009

Indium and nitrogen codoping in ZnO leads to a solid solution of InN in ZnO with a composition of $(Zn_{1-z}In_z)(O_{1-x}N_x)$. A simple solution combustion method has been adopted to prepare the above materials in less than 10 min with metal nitrates as the metal ion source and urea as fuel. With reference to ZnO, significant increase in lattice parameters was observed with increasing In-content. However, the In_2O_3 phase was observed along with InN for In content ≥10%. Optical absorption extended into the visible region, at least up to 550 nm, demonstrates an effective reduction of optical band gap due to the formation of solid solution. A new feature observed just above O 2p valence band in X-ray photoelectron spectroscopy (XPS) suggests the creation of N 2p states from InN; the N 1s core level XPS result too confirms nitride contribution. Raman spectroscopy and secondary ion mass spectrometry results show direct In−N, Zn−N, and In−N−Zn fragments in $(Zn_{1-z}In_z)(O_{1-x}N_x)$. Catalytic activity explored for oxidation of 2-butanol to ethyl methyl ketone demonstrates a high selectivity at 350 and 400 °C. All of the above characteristics suggest the multifunctional nature of $(Zn_{1-z}In_z)(O_{1-x}N_x)$ and its potential for other applications.

1. Introduction

The importance of ZnO in gas sensing to UV light emitters and ceramics is well-known, and recent reviews highlight the untapped potential and the problems associated with ZnO.[1] Due to its unique properties, ZnO finds many applications in commercially important reactions or products, such as reforming, methanol synthesis, or sun-blockers, etc.[2] In order to explore better potential associated with ZnO, suitable doping is required to achieve the desired activity from both a physical and chemical application point of view. Doping in the ZnO lattice, either in the place of Zn or O, helps reach many sophisticated applications in better way, as its electronic properties and electronic structure can be modified significantly. Although nitrogen has been considered as the best candidate for *p*-type doping for ZnO, however, the *p*-type behavior reported for N doped ZnO ($ZnO_{1-x}N_x$) is not fully reproducible, and controversies still exist.[3] In spite of the different sources of nitrogen used (NH_3, N_2, N_2O) and various sophisticated preparation methods employed, reproducible methods were not available to prepare $ZnO_{1-x}N_x$ due to the low nitrogen solubility in ZnO. Further, N-doping creates a deep acceptor level, which is unfavorable to induce *p*-type conductivity. Therefore, it is necessary to find methods that can enhance the solubility limit of N in ZnO. Recently, we reported a solution combustion method (SCM) to introduce large atom percents of N (up to 15%) in the ZnO lattice,[4] but without *p*-type conductivity, since N 2p states are found to be in the forbidden gap. Further, the charge density of N on $ZnO_{1-x}N_x$ is not as in any typical nitride, but resembles that of ammonia.[4]

The codoping method was followed to change the status of nitrogen into nitride. For this purpose, incorporation of both donor (Al, Ga, In) and acceptor (N, P, As) via codoping was suggested since group III metals

*Author to whom correspondence should be addressed. Phone: 0091-20-2590 2043. Fax: 0091-20-2590 2633. E-mail: cs.gopinath@ncl.res.in. Web site: www.ncl.org.in/csgopinath.

(1) (a) Klingshirn, C. *Chem. Phys. Chem.* **2007**, *8*, 782. (b) Özgür, Ü.; Alivov, Y. I.; Liu, C.; Teke, A.; Reshchikov, M. A.; Dogan, S.; Avrutin, V.; Cho, S. J.; Morkoc, H. *J. Appl. Phys.* **2005**, *98*, 041301.
(2) (a) Velu, S.; Suzuki, K.; Gopinath, C. S. *J. Phys. Chem. B* **2002**, *106*, 12737. (b) Melian-Cabrera, I.; Lopez Granados, M.; Terreros, P.; Fierro, J. L. G. *Catal. Today* **1998**, *45*, 251. (c) Mishra, B. G.; Ranga Rao, G. *J. Mol. Catal. A* **2006**, *243*, 204. (d) Bhanage, B. M.; Fujita, S.; Ikushima, Y.; Arai, M. *Green Chem.* **2003**, *5*, 429. (e) Vijayaraj, M.; Gopinath, C. S. *J. Catal.* **2006**, *241*, 83. (f) Velu, S.; Suzuki, K.; Gopinath, C. S.; Hattori, T.; Yoshida, H. *Phys. Chem. Chem. Phys.* **2002**, *4*, 1990.
(3) (a) Iwata, K.; Fons, P.; Yamada, A.; Matsubara, K.; Niki, S. *J. Cryst. Growth* **2000**, *209*, 526. (b) Guo, X.-L.; Tabata, H.; Kawai, T. *J. Cryst. Growth* **2002**, *237*, 544. (c) Yamauchi, S.; Goto, Y.; Hariu, T. *J. Cryst. Growth* **2004**, *260*, 1. (d) Look, D. C.; Reynolds, D. C.; Litton, C. W.; Jones, R. L.; Eason, D. B.; Cantwell, G. *Appl. Phys. Lett.* **2002**, *81*, 1830. (e) Xiong, G.; Wilkinson, J.; Mischuck, B.; Tuzemen, S.; Ucer, K. B.; Williams, R. T. *Appl. Phys. Lett.* **2002**, *80*, 1195. (f) Perkins, C. L.; Lee, S. H.; Li, X.; Asher, S. E.; Coutts, T. J. *J. Appl. Phys.* **2005**, *97*, 034907.
(4) Mapa, M.; Gopinath, C. S. *Chem. Mater.* **2009**, *21*, 351.

Published on Web 12/17/2009

have a stronger affinity toward N than Zn.[5] On the basis of this approach, experimental studies have been performed to enhance the nitride content, and there is limited success with thin-film materials prepared by various methods, especially in increasing nitrogen solubility.[5] Our recent studies[6] on codoping of Ga and N in ZnO lead to a solid solution of nanoclusters of GaN in ZnO with a significant decrease in the optical band gap up to 2.5 eV, from 3.37 eV for ZnO. In addition, the above method also stabilizes a good amount of nitrogen as nitrides. However, unlike Ga and N codoping, very few reports are available on codoping of In and N in ZnO. Chen et al.[7a,b] recently reported on the synthesis of *p*-type ZnO films by means of In and N codoping, and a hole density around 10^{18} cm^{-3} has been reported.[7c]

Although In^{3+} (0.84 Å) is considerably bigger than Zn^{2+} (0.72 Å), Zn could be substituted by In due to the structural similarity, and InN possess the same hexagonal wurtzite crystal structure (a = 3.537 Å, c = 5.704 Å) as that of ZnO (a = 3.250 Å, c = 5.205 Å); however, the band gap of InN is 0.7 eV,[8] compared to 3.37 eV for ZnO. Further, there is void space available in the wurtzite (B4) structure makes it feasible to accommodate bigger ions. In view of this, if In could be doped successfully, then the chances of forming a solid solution of InN in ZnO is very significant. At present, the III−V nitride compounds, such as AlN, GaN, and InN and N-doping in oxides, particularly TiO_2 have received considerable interest because of their potential applications in microelectronic and optoelectronic devices, and they are chemically and mechanically stable.[9] The codoping technique is an effective approach in producing *p*-type ZnO, regardless of Al−N, Ga−N, or In−N pairs.[5,6]

In the present study, up to 16 at % nitrogen was introduced with up to 10 at % In into ZnO as InN through SCM. SCM is an alternative synthetic method for producing a wide variety of simple and complex inorganic materials having excellent physicochemical properties. The method is gaining increased interest for the preparation of variety of materials, such as, nitrides, carbides, many composite materials, to enhance metal ion distribution on oxides, etc.[10] In the present case, the resulting solid solution of InN in ZnO, $(Zn_{1-z}In_z)(O_{1-x}N_x)$, exhibits an electronic structure that is markedly different from ZnO and InN. Indeed $(Zn_{1-z}In_z)(O_{1-x}N_x)$ materials exhibit an optical band gap of about 2.3 eV due to the N 2p states, from nitride, occupying the states above O 2p valence band. The above materials have been characterized by various physicochemical, microscopic, spectroscopic, and structural methods; further alcohol dehydrogenation reaction, without any acceptors, was explored via a heterogeneous catalysis. Indeed the results suggest the multifunctional nature of $(Zn_{1-z}In_z)(O_{1-x}N_x)$ materials. The present work is a part of our ongoing studies on N-doping in metal oxides toward making materials for various applications, including photocatalysis.[4,6,9h−k]

2. Experimental Section

2.1. Preparation of $(Zn_{1-z}In_z)(O_{1-x}N_x)$ Materials. All the chemicals employed were of analytical grade and used as such without any purification. $Zn(NO_3)_2 \cdot 6H_2O$ (Merck) as zinc precursor, $In(NO_3)_3$ as In source (Sigma-Aldrich), and urea (Merck) as fuel were used. In any typical synthesis of $(Zn_{1-z}In_z)(O_{1-x}N_x)$ material, the fuel to metal molar ratio [urea/(Zn + In)] was maintained at either 3, 5, or 7 with required Zn + In composition, and In atom % varied from 2 to 15. Required metal nitrate and urea were taken in a 250 mL beaker with 10 mL of distilled water. The above mixture was stirred until a uniform solution occurs and then introduced into a muffle furnace maintained at 500 °C. Water evaporates in the first few minutes followed by ignition of the reactant mixture yielding a solid $(Zn_{1-z}In_z)(O_{1-x}N_x)$ material. The solid product was collected after the completion of the combustion process. Selected materials were also calcined at 500 and 800 °C for 4 h to explore on the thermal stability. In-content at >10% shows In_2O_3 as an impurity in the above materials, and hence, they are not discussed here.

2.2. Characterization Methods. Powder X-ray diffraction (XRD) data of $(Zn_{1-z}In_z)(O_{1-x}N_x)$ materials was collected on a Rigaku X-ray diffractometer (DMAX IIIVC) equipped with Ni-filtered Cu Kα radiation (λ = 1.542 Å) and graphite crystal monochromator. Selected samples of XRD data were collected on Philips X'Pert Pro diffractometer. The data were collected with a step size of 0.020° and a scan rate of 0.50°/min.[11] The

(5) (a) Sato, K.; Katayama-Yoshida, H *Jpn. J. Appl. Phys.* **2007**, *46*, L1120. (b) Yamamoto, T.; Hiroshi, K Y. *Physica B* **2001**, *302−303*, 155. (c) Yamamoto, T. *Thin Solid Films* **2002**, *420−421*, 100. (d) Singh, A. V.; Mehra, R. M.; Wakahara, A.; Yoshida, A. *J. Appl. Phys.* **2003**, *93*, 396. (e) Ohshima, T.; Ikegami, T.; Edihara, K; Thareja, A. R. *Thin Solid Films* **2003**, *435*, 49.
(6) Mapa, M.; Thushara, K. S.; Saha, B.; Chakraborty, P.; Janet, C. M.; Viswanath, R. P.; Nair, C. M.; Murty, K. V. G. K.; Gopinath, C. S. *Chem. Mater.* **2009**, *21*, 2973.
(7) (a) Chen, L. L.; Lu, J. G.; Ye, Z. Z.; Lin, Y. M.; Zhao, B. H.; Ye, Y. M.; Li, J. S.; Zhu, L. P. *Appl. Phys. Lett.* **2005**, *87*, 252106. (b) Chen, L. L.; Yea, Z. Z.; Lu, J. G.; Chu, K. P. *Appl. Phys. Lett.* **2006**, *89*, 252113. (c) Kong, J. F.; Chen, H.; Ye, H. B.; Shen, W. Z.; Zhao, J. L.; Li, X. M. *Appl. Phys. Lett.* **2007**, *90*, 041907.
(8) (a) http://www.ioffe.rssi.ru/SVA/NSM/Semicond/InN/basic.html (accessed April 2009). (b) Wu, J.; Walukiewicz, W.; Yu, K. M.; Ager, J. W.III; Haller, E. E.; Lu, H.; Schaff, W. J. *Appl. Phys. Lett.* **2002**, *80*, 4741.
(9) (a) Jain, S. C.; Willander, M.; Narayan, J.; Overstraeten, R. V. *J. Appl. Phys.* **2000**, *87*, 956.(b) III-V Nitrides. *MRS Symposium Proceedings*; Ponac, F. A., Moustakas, T. D., Akasaki, I., Monemar, B. A., Eds.; MRS: Pittsburgh, 1997; Vol. *449*. (c) Morkoc, H.; Strite, S.; Gao, G. B.; Lin, M. E.; Sverdlov, B.; Burns, M. *J. Appl. Phys.* **1994**, *76*, 1263. (d) Nakamura, S.; Mukai, T.; Senoh, M. *Appl. Phys. Lett.* **1994**, *64*, 1687. (e) Wu, J.; Walukiewicz, W.; Yu, K. M.; Ager, J. W.; Haller, E. E.; Lu, H.; Schaff, W. J.; Saito, Y.; Nanishi, Y. *Appl. Phys. Lett.* **2002**, *80*, 3967. (f) Asahi, R.; Morikawa, T.; Ohwaki, T.; Aoki, K.; Taga, Y. *Science* **2001**, *293*, 269. (g) Buha, J.; Djerdj, I.; Antonietti, M.; Niederberger, M. *Chem. Mater.* **2007**, *19*, 3499. (h) Sathish, M.; Viswanath, R. P.; Gopinath, C. S. *Chem. Mater.* **2005**, *17*, 6349. (i) Sathish, M.; Viswanath, R. P.; Gopinath, C. S. *J. Nanosci. Nanotech.* **2009**, *9*, 423. (j) Gopinath, C. S. *J. Phys. Chem. B* **2006**, *110*, 7079. (k) Kulkarni, D. G.; Murugan, A. V.; Kasi Viswanath, A.; Gopinath, C. S. *J. Nanosci. Nanotech.* **2009**, *9*, 371.
(10) (a) Patil, K. C.; Arunab, S. T.; Mimania, T. *Curr. Opin. Sol. State Mater. Sci.* **2002**, *6*, 507. (b) Murugan, B.; Srinivas, D.; Gopinath, C. S.; Ramaswamy, V.; Ramaswamy, A. V. *Chem. Mater.* **2005**, *17*, 3983. (c) Murugan, B.; Ramaswamy, A. V.; Srinivas, D.; Gopinath, C. S.; Ramaswamy, V. *Acta Mater.* **2008**, *56*, 1461. (d) Bera, P.; Priolkar, K. R.; Gayen, A.; Sarode, P. R.; Hegde, M. S.; Emura, S.; Kumashiro, R.; Jayaram, V.; Subbanna, G. N. *Chem. Mater.* **2003**, *15*, 2049. (e) Bera, P.; Patil, K. C.; Jayaram, V.; Hegde, M. S.; Subbanna, G. N. *J. Mater. Chem.* **1999**, *9*, 1801. (f) Bera, P.; Patil, K. C.; Jayaram, V.; Hegde, M. S.; Subbanna, G. N. *J. Catal.* **2000**, *196*, 293.
(11) (a) Joly, V. L. J.; Joy, P. A.; Date, S. K.; Gopinath, C. S. *J. Phys. Cond. Matt.* **2001**, *13*, 649. (b) Mathew, T.; Rao, B. S.; Gopinath, C. S. *J. Catal.* **2004**, *222*, 107. (c) Vijayaraj, M.; Gopinath, C. S. *J. Catal.* **2006**, *243*, 376. (d) Shiju, N. R.; Anilkumar, M.; Mirajkar, S. P.; Gopinath, C. S.; Satyanarayana, C. V.; Rao, B. S. *J. Catal.* **2005**, *230*, 484.

Table 1. Physicochemical Characteristics of $(Zn_{1-z}In_z)(O_{1-x}N_x)$ Materials

material code[a,b]	surface area (m^2/g)	a (Å)	c (Å)
UZ5In2—$Zn_{0.98}In_{0.02}O_{0.91-\delta}N_{0.09}$	7	3.25258(2)	5.2080(2)
UZ5In5—$Zn_{0.95}In_{0.05}O_{0.88-\delta}N_{0.12}$	10	3.25515(6)	5.2103(8)
UZ5In8—$Zn_{0.92}In_{0.08}O_{0.85-\delta}N_{0.15}$	18	3.26203(5)	5.2132(2)
UZ5In10—$Zn_{0.9}In_{0.1}O_{0.84-\delta}N_{0.16}$	22	3.26555(8)	5.2150(5)
UZ5—$ZnO_{0.914-\delta}N_{0.086}$	7	3.2421(5)	5.1924(2)
UZ7—$ZnO_{0.93-\delta}N_{0.071}$	19	3.2414(7)	5.1934(4)
ZnO	40	3.250	5.205
InN		3.533	5.693

[a] Urea/(Zn + In) molar ratio and In atom percent is given after "UZ" and In, respectively, in material codes. δ indicates oxygen vacancy, and it could be up to 0.02. [b] Bulk atomic content and materials composition measured from energy-dispersive X-ray analysis (EDX) and chemical analysis.[12]

observed interplanar d spacing was corrected with reference to Si. Rietveld refinement of the selected powder XRD profiles was carried out using the X'Pert Plus software. The standard deviation of the least-squares fit of an observed intensity profile was typically $\leq 0.002°$ 2θ.

Surface area of the samples was estimated by N_2-adsorption/desorption isotherms, measured at −196 °C (NOVA 1200 Quanta Chrome equipment). Scanning electron microscopy (SEM) and energy dispersive X-ray (EDX) measurements were performed on an SEM system (Leica, Model Stereoscan-440) equipped with a recently installed EDX analyzer (Bruker, D451-10C Quantax 200 with X-flash detector) attachment. The X-flash 4010 detector was employed for fast and high resolution real time spectrometry and elemental mapping over large area of specimens. EDX spectra were recorded in the spot-profile mode by focusing the electron beam onto specific regions of the sample. However the materials composition reported in this communication is based on the data collected over large areas ($> 300\,\mu m^2$), and it is also in agreement with chemical analysis of metal ions. Calibration experiment for nitrogen estimation was measured with mixtures of GaN and silica.[4,6,11] Quantitative chemical analysis of metal ions (Zn and In) content was carried out with standard Vogel's procedure[12] by acid digestion of $(Zn_{1-z}In_z)(O_{1-x}N_x)$ materials followed by required dilution and titration with (ethylenedinitrilo) tetraacetic acid (EDTA). This provides the total amount of Zn + In content, since both the metal ions are equally reactive to EDTA. However titration of the acid-digested solution, after adjusting the pH to 7−8 with the addition of acid-buffer (acetic acid and ammonium acetate), with KCN leads to zinc cyanide complex formation and gives the exact values of Zn-content.[12b] This is mainly to eliminate any interference from In and more details are available in ref 12b. In-content has been obtained by subtracting the Zn-content from the EDTA measured value. Further the acid-digested solution was subjected to inductively coupled plasma analysis to reconfirm the metal ion contents. Metal ion-contents measured by the above methods also corroborate well with EDX analysis and further increases the confidence level of composition reported in Table 1. Thermal analysis experiments were measured in Perkin-Elmer's Diamond TG/DTA at a rate of 10 °C/min in air or N_2 atmosphere.[11]

Diffuse reflectance UV−vis measurements were carried out on a Shimadzu spectrophotometer (model UV-2550) with spectral-grade $BaSO_4$ as reference material. Raman spectra were recorded on a Horiba JY LabRAM HR 800 Raman spectrometer coupled with microscope in reflectance mode with 633 nm excitation laser source and a spectral resolution of 0.3 cm^{-1}. X-ray photoelectron spectra (XPS) were recorded on VG Microtech Multilab ESCA 3000 spectrometer equipped with Al Kα (1486.6 eV) or Mg Kα (1253.6 eV) X-ray sources. Selected spectra, especially N 1s and valence band spectra were recorded with both the above sources to eliminate the overlap between different Auger and/or core levels. Base pressure in the analysis chamber was maintained in the range of $3-6 \times 10^{-10}$ Torr. Binding energy (BE) calibration was performed with Au $4f_{7/2}$ core level at 83.9 eV.[11] Secondary ion mass spectrometry (SIMS) studies were carried out with a QMS-based instrument (Hiden Analytical). Bombardment was done with 5 keV oxygen and cesium ions. The primary ion current was 400 nA (oxygen beam) and 100 nA (cesium beam). The beam was rastered over an area of 1000 μm^2; however, the secondary ions were collected from the central 200 μm^2 area.[6]

2.3. Catalytic Reactor. Vapor phase dehydrogenation of 2-butanol was carried out at atmospheric pressure in a fixed bed, vertical downflow, glass reactor placed inside a double zone furnace (Geomechanique, France).[11] Fresh catalyst (1.0 g) with particle size up to 10 mesh was charged each time in the center of the reactor in such a way that the catalyst was sandwiched between the layers of inert glass beads. The reactant was fed using a syringe pump at a weight hourly space velocity (WHSV) of 5. Reaction products were collected at ice cold conditions from a condenser fixed below the reactor and analyzed by an Agilent Gas Chromatograph (19091J-413) containing an HP 5.5% phenyl methyl siloxane column equipped with a flame ionization detector. Gaseous and liquid products were also analyzed using GC-MS.[11c]

3. Results and Discussion

Throughout the manuscript, $ZnO_{1-x}N_x$ and $(Zn_{1-z}In_z)(O_{1-x}N_x)$ materials are denoted as UZx and UZxIny, respectively, with x and y being the ratio of urea/(Zn + In) and In atom %, respectively, unless otherwise specified. A list of relevant $ZnO_{1-x}N_x$ and $(Zn_{1-z}In_z)(O_{1-x}N_x)$ materials that were prepared, via SCM, is given in Table 1 with some physicochemical properties. On $ZnO_{1-x}N_x$ materials, the chemical state of nitrogen is as that of ammonia, and it has been discussed with other characteristics in our earlier communication;[4] however, nitrogen codoped with In leads to a solid solution of InN in ZnO.

3.1. X-ray Diffraction. Figure 1 shows the characteristic XRD patterns of various materials $(Zn_{1-z}In_z)(O_{1-x}N_x)$ synthesized in the present investigation and compared with $ZnO_{1-x}N_x$, ZnO, InN, and In_2O_3. Figure 1a shows the XRD patterns obtained with different ratios of urea/(Zn + In) (3, 5, and 7) with In = 5 atom %. The XRD pattern of pure ZnO and InN shows a hexagonal wurtzite structure. A sharp and well-refined ZnO

(12) (a) *Vogel's textbook of Quantitative Inorganic Analysis*; Mendham, J., Denney, R. C., Barnes, J. D., Thomas, M. J. K., Eds.; Prentice-Hall: Harlow, England, 2000. (b) Cheng, K. L. *Anal. Chem.* **1955**, *27*, 1582.

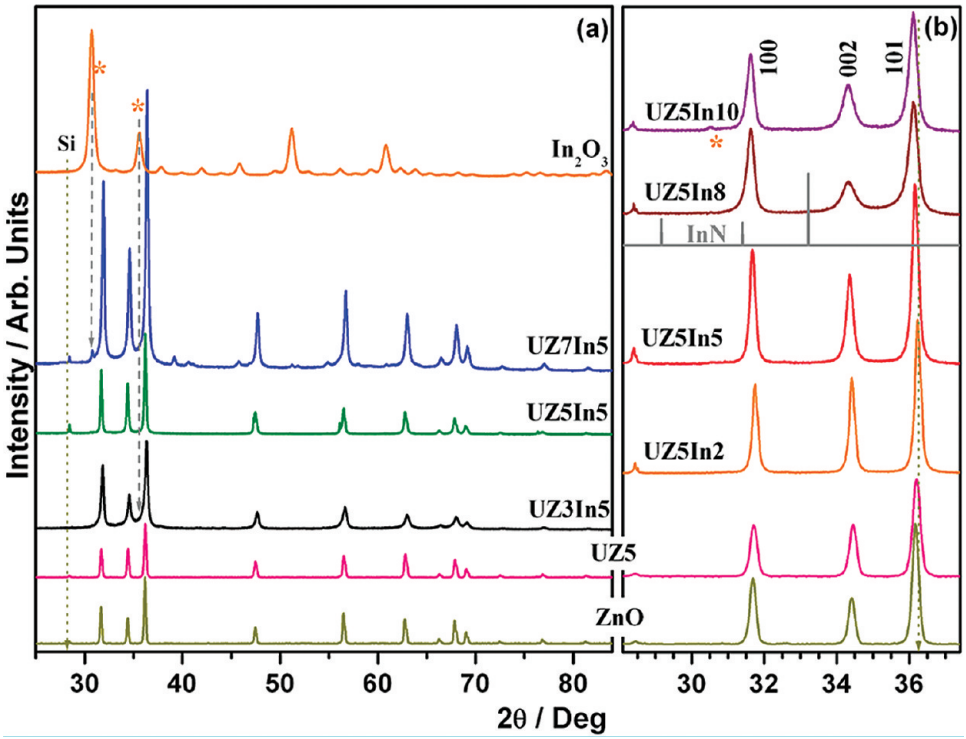

Figure 1. Powder X-ray diffraction pattern of (a) $(Zn_{0.95}In_{0.05})(O_{1-x}N_x)$, prepared with urea/(Zn + In) = 3, 5, and 7, and (b) $(Zn_{1-z}In_z)(O_{1-x}N_x)$ prepared with urea/(Zn + In) = 5 and In-content between 0 and 10 atom %. UZ5, In_2O_3, InN, and ZnO are also plotted for comparison. Si has been used as an internal standard and indicated by a dotted line. Dashed lines and * symbols indicate the contribution due to In_2O_3.

pattern is observed for UZ5In5. However, there is significant peak broadening observed for both UZ3In5 and UZ7In5 with an In_2O_3 feature clearly observed at $2\theta = 30.76°$ (JCPDS data card No. 71-2194) on the latter material. In_2O_3 features were also observed for materials prepared with In percents higher than 5 with a urea/(Zn + In) ratio other than 5. In view of this observation, most of the results have been presented from UZ5In*y*, unless specified. Nevertheless, no reflections other than those corresponding to the host ZnO matrix are observed in these XRD patterns; especially no peaks corresponding to impurities such as In_2O_3 and $ZnIn_2O_4$ are observed up to In = 10 atom %. It is worth noting that the as-prepared In-containing materials are highly crystalline (Figure 1), attesting the effectiveness of the SCM to induce in situ crystallization during the material formation. It is also to be underscored that the actual combustion time is less than 1 min, although the entire preparation requires about 8−10 min. Time required for initial drying of the aqueous reaction mixture was a few minutes, followed by increase in the temperature of the solid mass and subsequent combustion. Indeed during the above combustion, in situ production of NH_3, due to urea decomposition, acts as the nitrogen source. Nascent zinc oxide clusters (Zn_aO_b with $a/b > 1$) with plenty of defects are very likely to interact with NH_3 to produce N-doped materials. Hence, this procedure might be used to incorporate nitrogen into most of the metal oxides.

Figure 1b shows the XRD patterns obtained from UZ5In*y* ($y \leq 10$) and compared with standard reference materials. Well-resolved high intensity reflections have been observed up to In = 8% without any impurity phases. However, with increasing In-content, the full width at half-maximum (FWHM) value of all the peak increases, implying a decreasing crystallite size due to incorporation of In and N into the ZnO lattice. Diffraction peaks also shift to lower 2θ with increasing In-content, and this is indicated by a dotted line. The lattice parameter "*a*" (*c*) value increases from 3.250 Å (5.205 Å) for pure ZnO to 3.26203 Å (5.2132 Å) for In = 8 atom % in $(Zn_{1-z}In_z)(O_{1-x}N_x)$ (Table 1). This suggests that In^{3+} (N^{3-}) replaces Zn^{2+} (O^{2-}) in the ZnO lattice with a concomitant increase in the lattice parameters due to larger size of In and N. This also indicates that the materials prepared are not physical mixtures of InN and ZnO, rather a solid solution of InN in ZnO. The XRD pattern of InN (Figure 1b) demonstrates that the broadening observed at high In-content (≥8%) is due to InN. It is likely that nanosized InN clusters might be dispersed homogeneously in the ZnO lattice system which can be attributed to the fact that there is no peak specific to InN observed, rather a shift to lower angle is observed. It is to be noted that, in the codoping of Ga and N in ZnO, formation of −N−Ga−N−Ga−N− clusters that occupy near-neighbor sites is favorable due to the strong attractive interaction between them and it helps to increase the solubility of N in ZnO.[13] In a very similar manner, we find evidence for nanosized −In−N−In−N− clusters from all analytical methods employed.

(13) (a) Yamamoto T.; Katayama-Yoshida, H, Jpn. J. Appl. Phys., Part 2 **1999**, *38*, L166. (b) Singh, A. V.; Mehra, R. M.; Wakahara, A.; Yoshida, A. *J. Appl. Phys.* **2003**, *93*, 396. (c) Ohshima, T.; Ikegami, T.; Edihara, K; Asmussen, J.; Thareja, R. *Thin Solid Films* **2003**, *435*, 49.

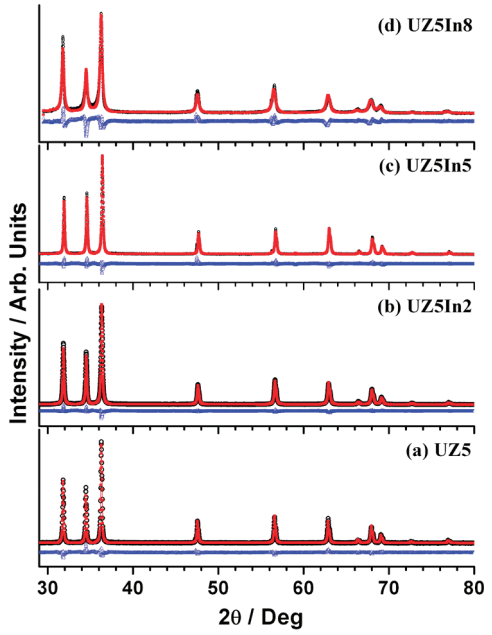

Figure 2. Rietveld refinement profiles of (a) UZ5, (b) UZ5In2, (c) UZ5In5, and (d) UZ5In8 $(Zn_{1-z}In_z)(O_{1-x}N_x)$ materials prepared by SCM. Experimental data points are given in open black circles, and calculated intensity is given in solid red squares. The difference plot is given in blue at the bottom.

Attempts to synthesize materials with higher In loadings leads to a mixed phase of $(Zn_{1-z}In_z)(O_{1-x}N_x)$ and In_2O_3. Reflection corresponding to In_2O_3 was observed for In % ≥ 10. A further urea to metal ratio of 7 and 3 employed also leads to an In_2O_3 phase, especially with In % > 5. Urea being a good fuel, complete combustion takes place and the average combustion temperature increases with urea content.[4,14] This underscores the necessity of optimum temperature for effective preparation of $(Zn_{1-z}In_z)(O_{1-x}N_x)$, which is achieved around urea/(Zn + In) = 5. Rietveld refinement profiles of materials prepared by SCM using urea/(Zn + In) = 5 with different In loadings are presented in Figure 2. An excellent agreement between the experimental and the fitted data indicated that the XRD pattern could be indexed reasonably well to the Wurtzite structure with a space group $P6_3mc$.

The positions of major ((100), (002), and (101)) diffraction peaks were successively shifted to lower angles (2θ) with increasing In content, indicating that the $(Zn_{1-z}In_z)(O_{1-x}N_x)$ materials were indeed solid solutions of InN in ZnO (Figure 1b). The peak shift is considerable, as the ionic radius of In^{3+} (0.84 Å) is higher than that of Zn^{2+} (0.72 Å).[15] However, the covalent bond length of In−N (~2.4 Å) is larger than that of Zn−O (1.97 Å), and In substituted at Zn sites would increase the lattice parameter as well as volume, thus justifying the peak shift

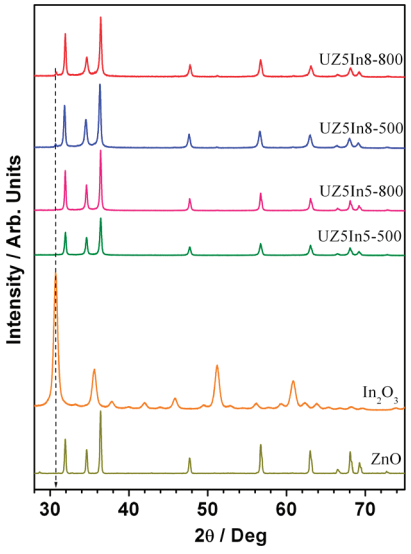

Figure 3. Powder X-ray diffraction pattern of calcined $(Zn_{1-z}In_z)$-$(O_{1-x}N_x)$ materials, prepared with urea/(Zn + In) = 5, and compared with In_2O_3 and ZnO.

to the lower angle. It is clear from the above observations that N and In atoms occupied the O and Zn lattice positions, respectively. It is also to be noted that the percent increase in the unit cell parameter *a* is significantly higher than "*c*" (Table 1) with increasing In-content, and the reason for this is not known. With increasing urea/(Zn + In) ratio from 5 to 7 in the combustion reaction mixture, a new peak appears at 2θ = 30.76° which indicate the formation of In_2O_3. Therefore, with increasing urea concentration, it is clear that a large amount of heat is produced[4] which is likely to oxidize InN to In_2O_3.

It is known that InN begins to decompose with loss of nitrogen between 425 and 550 °C.[16] To explore on the stability of the $(Zn_{1-z}In_z)(O_{1-x}N_x)$ materials prepared, calcination at different temperatures and thermal analysis experiments was performed. As already indicated, the materials prepared by SCM get exposed to high temperatures during synthesis and hence a better thermal stability is expected. Indeed the XRD pattern measured for UZ5In5 after calcination at 500 and 800 °C does not show any impurity peaks (Figure 3); however, UZ5In8 exhibits an additional peak at 2θ = 30.76° and a clear peak broadening at 36.5° was observed. Above new features are attributed due to the formation of In_2O_3. Due to calcination in static air, InN gets oxidized to In_2O_3 which does not belong to the wurtzite phase and reflects in the XRD patterns. However with In-content ≤5%, no formation of In_2O_3 was observed, indicating that the smaller InN clusters might be stable and resistant to oxidation, at least, up to 500 °C.

Apart from InN, a significant amount of excess nitrogen in $(Zn_{1-z}In_z)(O_{1-x}N_x)$ materials leads to a question

(14) (a) Deshpande, K.; Mukasyan, A.; Varma, A. *Chem. Mater.* **2004**, *16*, 4896. (b) Hwang, C.-C.; Wu, T.-Y. *J. Mater. Sci.* **2004**, *39*, 6111. (c) Lenka, R. K.; Mahata, T.; Sinha, P. K.; Tyagi, A. K. *J. Alloys Comp.* **2008**, 466 326.(d) Mapa, M. Synthesis, characterization and catalytic studies of heteroatoms incorporated ZnO. Ph.D. Thesis. University of Pune, **2009**.
(15) (a) Dingman, S. D.; Rath, N. P.; Markowitz, P. D.; Gibbons, P. C.; Buhro, W. E. *Angew. Chem. Intern. Ed.* **2009**, *39*, 1470. (b) Tzeng, Y.-R.; Raghunath, P.; Chen, S.-C.; Lin, M. C. *J. Phys. Chem. A.* **2007**, *111*, 6781.
(16) (a) Neumayer, D. A.; Ekerdt, J. G. *Chem. Mater.* **1996**, *8*, 9. (b) Jones, A. C.; Whitehouse, C. R; Roberts, J. S. *Chem. Vap. Deposition* **1995**, *1*, 65. (c) Akasaki, I.; Amano, H. *J. Cryst. Growth* **1995**, *146*, 455. (d) Grzegory, I.; Jun, J.; Bockowski, M.; Krukowski, St.; Wroblewski, M.; Lucznik, B.; Porowski, S. *J. Phys. Chem. Solids* **1995**, *56*, 639.

of the charge compensation mechanism in this type of material. Indeed, interstitial Zn and oxygen vacancies present in these materials[4] are evident from electron paramagnetic resonance (EPR) studies (see the Supporting Information, Figure SI-1). Indeed the interstitial Zn-content decreases and oxygen vacancies increase with increasing In-content from UZ5 to UZ5In5. This indicates the charge compensation mechanism in In-containing materials is mostly due to oxygen vacancies and to a lesser extent by interstitial Zn. Density values observed for UZ5 are comparable to that of ZnO suggesting the amount of interstitial Zn is negligible.

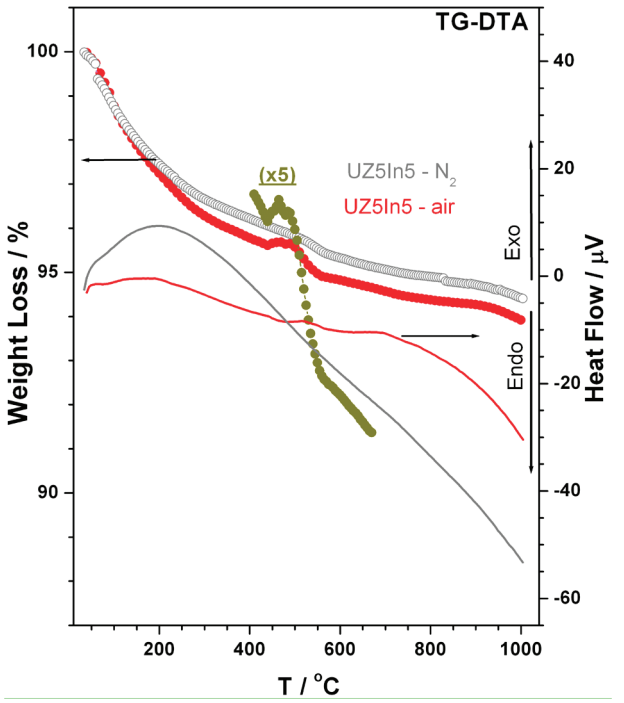

Figure 4. Thermogravimetric and differential thermal analysis of UZ5In5 carried out in air and nitrogen atmospheres. The weight gain observed on UZ5In5 around 500 °C (feature multiplied 5 times for clarity) in air atmosphere supports the oxidation of InN to In_2O_3. The same color has been used for TG and DTA.

3.2. Thermal Analysis. It is necessary to understand the oxidation mechanism of InN in $(Zn_{1-z}In_z)(O_{1-x}N_x)$ materials at high temperatures in air and N_2 atmosphere, mainly to understand its thermal stability. The oxidation process of pure InN films is rather complicated since the oxygen incorporation and the nitrogen desorption occur simultaneously.[17] During this process, InN oxidizes to cubic bixbyite In_2O_3 phase. Thermal analysis of UZ5In5 was carried out in simulated air atmosphere up to 1000 °C, and the results are shown in Figure 4. Interestingly, a mild weight gain (shown by 5× data points and shifted down vertically) was observed between 500 and 550 °C. This is attributed to the oxidation of InN to In_2O_3. To validate this conclusion, a similar experiment has been carried out in an N_2 atmosphere. The fact that the thermogravimetric differential thermal analysis (TG/DTA) result from UZ5In5 in an N_2 atmosphere does not show any weight gain around 500 °C supports the above conclusion. On quantification, a weight gain of 0.41(±0.08)% was measured, and it reiterates that the amount of InN is 5 mol %. For oxidation of 1 mol of bulk InN to 0.5 mol In_2O_3, a weight gain of 7.76% is expected, and hence, a weight gain with the above value of 0.41% fully supports 5 ± 0.5% InN in UZ5In5. Considerable weight loss observed < 400 °C due to the loss of physisorbed H_2O and possible nitrate decomposition on all samples. Nonetheless, after calcination to high temperatures around 800 °C, none of the $(Zn_{1-z}In_z)(O_{1-x}N_x)$ materials show any nitrogen, and

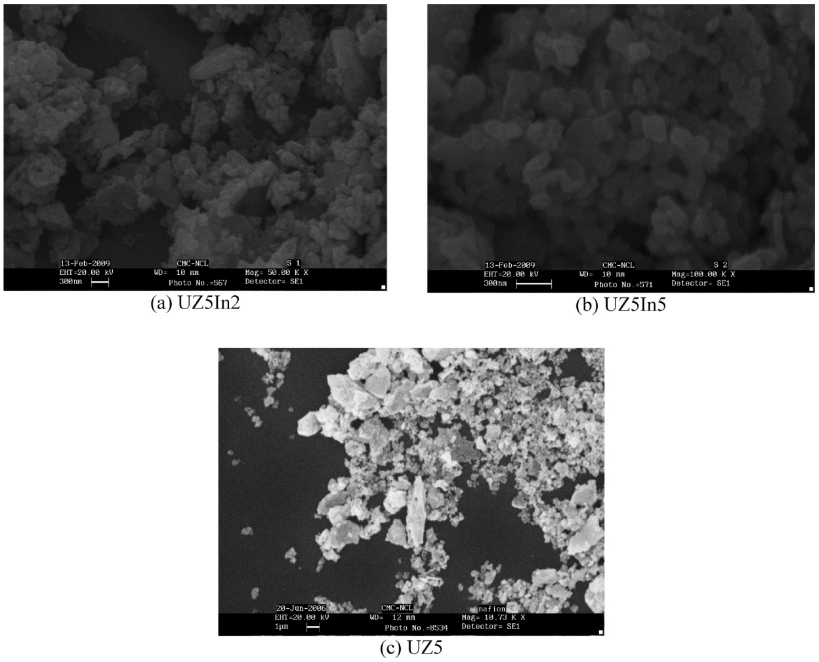

(a) UZ5In2 (b) UZ5In5

(c) UZ5

Figure 5. SEM images of as prepared $(Zn_{1-z}In_z)(O_{1-x}N_x)$ materials with In = (a) 2% and (b) 5%. All materials show an average particle size around 250 nm. (c) SEM image obtained from UZ5 which does not show any notable feature, suggesting that the In and N codoping leads to significant particle size ordering.

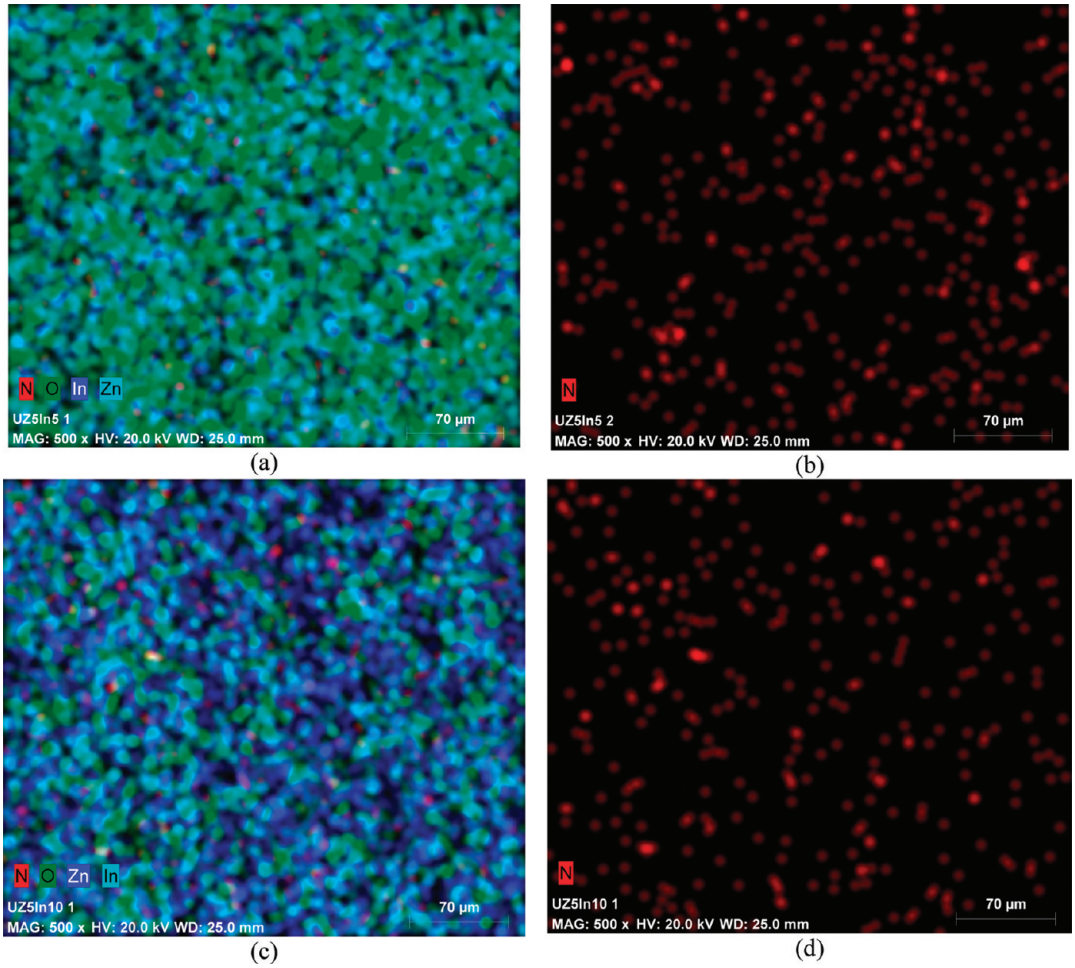

Figure 6. Elemental mapping of $(Zn_{1-z}In_z)(O_{1-x}N_x)$ materials (a and b) UZ5In5 and (c and d) UZ5In10 for (a and c) all constituent elements and (b and d) nitrogen, respectively. Color coding for different elements are shown on the images. The uniform distribution of In and N can be seen on all images over the large area of $360 \times 310\,\mu m^2$. Change in color from predominantly fluorescent green on panel a, to predominantly blue (+ cyan) on panel c suggests a change in surface composition from predominantly ZnO to ZnO + InN, respectively. An increase in N-content is also evident from panels b to d, while increasing the In-content from 5 to 10%.

this is affirmed by the XPS/EDX results. The fact that, with increase in In-content, weight loss also increases proves that there is a greater amount of nitrogen introduction with higher In percent. No In_2O_3 feature observed in XRD on UZ5In5 after heating at 800 °C might be due to smaller In_2O_3 cluster sizes; however, InN is thermally stable up to 500 °C on all UZ5Iny ($y \leq 10$) compositions.

3.3. Textural Properties. The morphology of the as prepared $(Zn_{1-z}In_z)(O_{1-x}N_x)$ materials was examined by SEM. Figure 5 shows representative SEM images of two $(Zn_{1-z}In_z)(O_{1-x}N_x)$ materials with UZ5In2 and UZ5In5. As-prepared materials exhibited a good distribution of fine primary particles with an average size of about 200−300 nm. However, some bigger particles were also observed. No specific particle shape was observed. UZ5 shows no particle morphology and a random size distribution (Figure 5c), in contrast to the predominant triangle/hexagonal prism shape for $ZnO_{1-x}N_x$ with N = 15%.[4] It is to be noted that a small percentage of In induces some ordering of particles, compared to complete random ordering on UZ5, and highlights significant changes in material preparation conditions. To find out the distribution of particle sizes, dynamic light scattering measurements have also been carried out with the above materials dispersed in an isopropanol solvent. It has been assumed that all of the particles are spherical in shape, and the results given in the Supporting Information (see Figure SI-2). The majority (95%) of particles from UZ5In5 exist in a size range between 230 and 330 nm, and the remaining (5%) show higher diameters between 1000 and 1200 nm. Both SEM and scattering experimental results are in good agreement with each other and confirm the nanosized regime of $(Zn_{1-z}In_z)(O_{1-x}N_x)$ materials, although the preparation method adopted was SCM, which involves high temperature between 700 and 1000 °C.

EDX analysis has been carried out to measure the material composition as well as to find out the extent of doping homogeneity. Representative results are given in Figure 6 for UZ5In5 (a and b), and UZ5In10 (c and d).

(17) (a) Bellosi, A.; Landi, E.; Tampieri, A. *J. Mater. Res.* **1993**, *8*, 565. (b) Katnani, A. D.; Papathomas, K. I. *J. Vac. Sci. Technol. A* **1987**, *5*, 1335. (c) Foley, C. P.; Lyngdal, J. *J. Vac. Sci. Technol. A* **1987**, *5*, 1708. (d) Westra, K. L.; Lawson, R. P. W.; Brett, M. J. *J. Vac. Sci. Technol. A* **1988**, *6*, 1730. (e) Lee, I. J.; Kim, J.-Y.; Hur, T.-B.; Kim, H.-K. *Phys. Stat. Sol. A* **2004**, *201*, 2777.

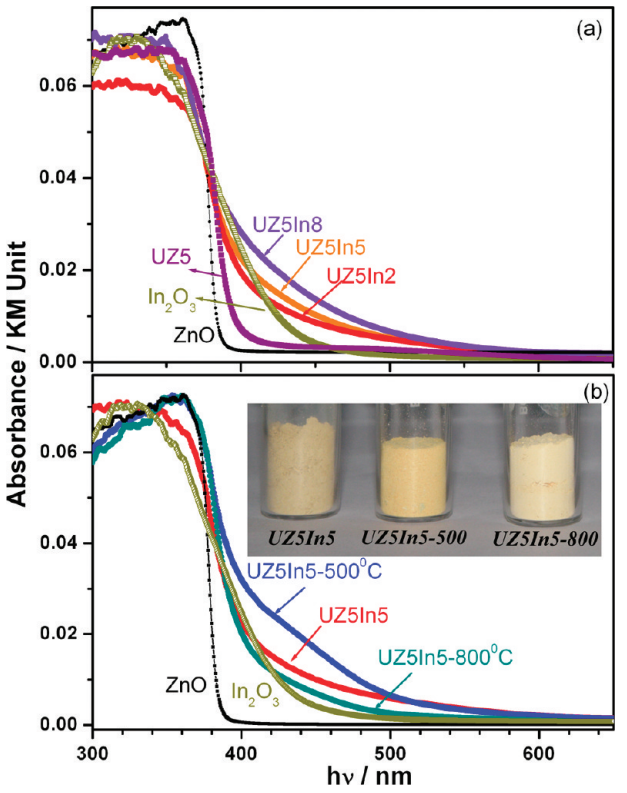

Figure 7. UV−visible absorption spectra of $(Zn_{1-z}In_z)(O_{1-x}N_x)$ materials prepared with urea/(Zn + In) = 5 for (a) different In-content and (b) after calcination at different temperatures for UZ5In5, and compared with In_2O_3 and ZnO. Color changes from the calcined materials are shown in the inset photograph.

Elemental mapping of all the elements have been carried out and shown with color coding for different elements. High intense and low intense (or diffused) color indicate the high and low content of corresponding elements, respectively, in a particular area/spot. Figure 6b and d shows only the nitrogen mapping of the above materials to show the homogeneous distribution over a large area (> 300 μm^2). First of all, the above results confirm the homogeneous distribution of doped elements at the microscopic level, indicating the effectiveness of the preparation method. It is also to be noted that the atom percent measured through EDX on individual particle differs significantly; however, values reported in Table 1 are the average values obtained over large areas (> 300 μm^2), as shown in Figure 6a and c. A glance at UZ5In5 (Figure 6a) and UZ5In10 (Figure 6c) highlights the change in surface composition from the former to the latter. An increase in In- and N-content on UZ5In10 compared to UZ5In5 is evident from Figure 6. Indeed, the red color (for N) could be seen better in Figure 6c than in Figure 6a. Although apparent N-distribution and content seems similar on both materials, quantitatively, it could not be shown in Figure 6 as the relative oxygen content did not change significantly. A careful look at the elemental map (Figure 6a and c) reveals the association of In and N preferentially to that of Zn and N, suggesting the solid solution of InN in ZnO. Further, the change in predominantly fluorescent green (and cyan) on UZ5In5 (Figure 6a) to blue + cyan (Zn + In) on UZ5In10 (Figure 6c) underscores the change in surface composition from predominantly ZnO on the former to ZnO + InN on the latter, respectively. Systematic color variation was observed with increasing In-content (not shown). It is also to be noted that our efforts to measure the N-content by Kjeldhal method with $(Zn_{1-z}In_z)(O_{1-x}N_x)$ and $ZnO_{1-x}N_x$ [4,6] materials did not give meaningful results, unlike with organic compounds and peptides. This is also a reason for the measurement of N-content primarily by analytical methods.

3.4. Optical Absorption. Optical absorption spectra of as prepared $(Zn_{1-z}In_z)(O_{1-x}N_x)$ and calcined materials have been measured, and the results compared with that of UZ5, In_2O_3, and ZnO (Figure 7). Pure ZnO shows a well-defined absorption cutoff edge at 380 nm; however, the pale greenish yellow In_2O_3 shows a gradual decrease in absorption from 370 to 440 nm.[18] A new visible absorption band with low intensity is observed at 480 nm on $ZnO_{1-x}N_x$ (UZ5) material. Our earlier studies[4,6] demonstrated the creation of a midgap state by N 2p states between valence band (VB) and conduction band (CB), and hence, there is no change in resistivity. Evidently, after doping In and N, visible light absorption onset is extended, at least, to 550 nm as shown in Figure 7a. Further, the new visible light absorption band of $(Zn_{1-z}In_z)(O_{1-x}N_x)$ materials, around 450 nm, shift to higher wavelength as well as the absorption coefficient increases with increasing In content up to 8%. There is a characteristic shift in color from pale greenish yellow for In_2O_3 to brown color $(Zn_{1-z}In_z)(O_{1-x}N_x)$, and it is unlikely there is any In_2O_3 in the codoped materials containing In < 10%. N and In codoping helps to form shallow donor and acceptor levels from N 2p and In 5s/5p and close to VB and CB, respectively, and effectively decreases the band gap by about 1 eV (to 2.3 eV). Our VB band studies with XPS demonstrate that nitride contributes to a large extent toward the band gap reduction, and this will be discussed later.

$(Zn_{1-z}In_z)(O_{1-x}N_x)$ materials were subjected to calcinations at different temperatures, and UV−vis absorption spectra were recorded subsequently. A representative result from UZ5In5 is given in Figure 7b. UZ5In5 calcined up to 400 °C (not shown) did not show significant changes in absorption characteristics compared to as prepared materials. However on calcination at 500 °C, there is a significant increase in absorption coefficient, and apparently, a new absorption band develops around 440−450 nm. Similar observation was recorded for UZ5In8 after calcinations at 500 °C. This new feature is not due to In_2O_3, since it exhibits absorption below 440 nm, but to a feature which is yet to be identified. However, on further calcination at temperatures > 500 °C, the above-mentioned new band disappears gradually, and the 800 °C calcined material shows a cut off edge as that of a physical mixture of ZnO and In_2O_3, since all InN was oxidized to In_2O_3. Indeed the color of UZ5In5 changes

(18) Kamata, K.; Maeda, K.; Lu, D.; Kako, Y.; Domen, K. *Chem. Phys. Lett.* **2009**, *470*, 90.

from dull brown to deep yellowish brown on calcination to 500 °C, which turns to a very pale yellow after calcination at 800 °C (see Figure 7b inset for change in material color). There is a good correspondence between the features in the visible light region for In_2O_3, and UZ5In5-800 °C demonstrates that all InN got oxidized to In_2O_3. As shown in XRD, UZ5In8-800 °C exhibits a new peak at $2\theta = 30.76°$ which corresponds to the In_2O_3 peak. Nevertheless, the important point is that the visible light absorption is exclusively due to two types of nitrogen that is combined with In and Zn.

There are few suggestions on the mechanism of band gap reduction by Inoue et al.[19] and Domen et al.,[20] especially on fully filled d^{10} systems (such as ZnO-, GaN-, and Ge_3N_4-based), such as p−d repulsion or p−d coupling responsible for shifting the VB maximum (VB_{max}) and hence a decrease in the band gap. For II−VI semiconductors, Wei and Zunger[21] pointed out that the p−d repulsion shifts the VB_{max} upward without affecting the CB minimum (CB_{min}). In the nitrides and oxides, the cation d states lie near the bottom of the VB and near the middle of the VB, respectively. In both cases the d states interact and hybridize with the states at the VB_{max}, which are comprised mostly of anion 2p states.[18,19] However, in the present $(Zn_{1-z}In_z)(O_{1-x}N_x)$ materials, it is unlikely that N/O 2p−In 4d repulsion plays any role, since the In 4d orbital is located as shallow core levels around 18 eV in VB and energetically far away from N 2p and/or O 2p orbitals. However, the possibility of lowering the CB_{min} is also to be considered, which is composed of Zn 4s/4p and In 5s/5p orbitals.[22] Nevertheless, the easy preparation of $(Zn_{1-z}In_z)(O_{1-x}N_x)$ materials underscores the chances of N/O 2p and Zn 4p and In 5p attraction (p−p attraction) and might be a factor to be considered for the band gap reduction mechanism. N 2p features observed in the VB support the above possibility and are worth exploring further.

3.5. Raman Spectroscopy. Figure 8 shows the Raman spectra of $(Zn_{1-z}In_z)(O_{1-x}N_x)$ with different In amounts and compared with ZnO and In_2O_3. ZnO exhibits a hexagonal wurtzite structure and belongs to the C_{6v} symmetry group with five Raman-active phonon

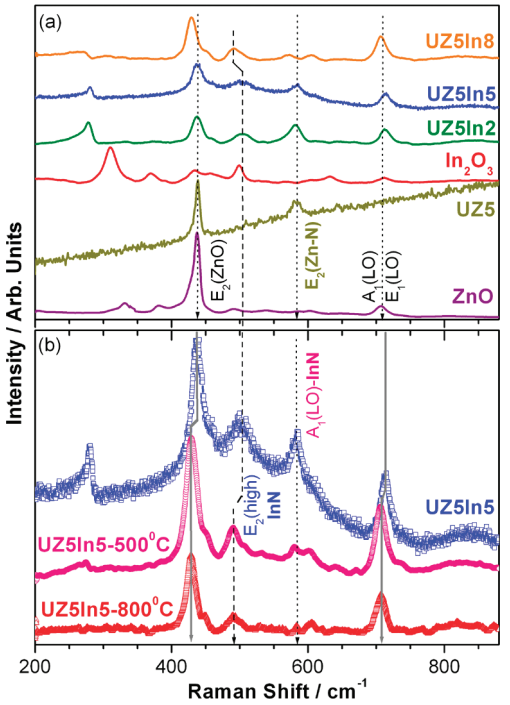

Figure 8. Raman spectra of (a) $(Zn_{1-z}In_z)(O_{1-x}N_x)$ materials with metal to urea ratio 5 and compared with ZnO, UZ5 and (b) UZ5In5, and the same after calcinations at 500 and 800 °C.

modes at 278, 381, 407, 437, 574, and 582 cm^{-1} for the A_1(TO), E_1(TO), E_2(high), A_1(LO), and E_1(LO) modes, respectively.[4,23] InN exhibits two strong optical phonons at 490 cm^{-1} (E_2(high)) and 583 cm^{-1} (A_1(LO)), which can be easily observed with common excitation sources.[7c,24]

A strong and sharp peak observed at 436 cm^{-1} on all $(Zn_{1-z}In_z)(O_{1-x}N_x)$ and ZnO is attributed to characteristic nonpolar E_2(high) phonons of the wurtzite structure. The phonon mode centered at 492 cm^{-1} on UZ5In8 is attributed to the E_2(high) mode of InN and in good agreement with literature reports;[24b,c] however, this phonon mode shifted to higher frequency (504 cm^{-1}) and broadened with lower In-content (2 and 5%), indicating the smaller cluster sizes of InN. The moderately intense peak at 582 cm^{-1} is attributed to longitudinal optical (A_1(LO) and E_1(LO)) phonon modes of $(Zn_{1-z}In_z)$-$(O_{1-x}N_x)$, especially for Zn−N as well as In−N related. This peak is not observed for pure ZnO; however, it is characteristic for typical nitrides, such as GaN, InN, and $ZnO_{1-x}N_x$.[4,6,23,24] The finding that E_2(high) and transverse optical (A_1(TO) at 382 cm^{-1}) modes of ZnO clearly weakened with an increase in In and N content in $(Zn_{1-z}In_z)(O_{1-x}N_x)$ supports the solid solution nature. In fact, all Zn−N and In−N related phonon mode intensities increased with In codoping. This is direct evidence to support the direct bonding between Zn/In and N in the $(Zn_{1-z}In_z)(O_{1-x}N_x)$ system. The A_1(LO) phonon mode of InN at 582 cm^{-1} overlaps with that of Zn−N related and difficult to resolve, since they appear at the same frequency. Interestingly, the E_2(high) of In_2O_3 observed at 303 cm^{-1} is not observed on $(Zn_{1-z}In_z)(O_{1-x}N_x)$ suggesting that the present codoping

(19) Inoue, Y. *Energy Environ. Sci.* **2009**, *2*, 364.
(20) Maeda, K.; Domen, K. *J. Phys. Chem. C* **2007**, *111*, 7851. (b) Osterloh, F. E. Chem. Mater. **2008**, *20*, 35 and references therein. (c) Maeda, K.; Teramura, K.; Takata, T.; Hara, M.; Saito, N.; Toda, K.; Inoue, Y.; Kobayashi, H.; Domen, K. *J. Phys. Chem. B* **2005**, *109*, 20504.
(21) Wei, S. H.; Zunger, A. *Phys. Rev. B* **1988**, *B37*, 8958.
(22) Sato, J.; Kobayashi, H.; Inoue, Y. *J. Phys. Chem. B.* **2003**, *107*, 7970.
(23) (a) Wang, D.; Seo, H. W.; Tin, C. C.; Bozack, M. J.; Williams, J. R.; Park, M.; Santhitsuksanoh, N.; Cheng, A.; Tzeng, Y. H. *J. Appl. Phys.* **2006**, *99*, 113509. (b) Haboeck, U.; Hoffmann, A.; Thomsen, C.; Zeuner, A.; Meyer, B. K. *Phys. Stat. Sol. B* **2005**, *242*, R21.
(24) (a) Kuball, M.; Pomeroya, J. W.; Wintrebert-Fouquet, M.; Butcher, K. S. A.; Lu, H.; Schaff, W. J. *J. Cryst. Growth* **2004**, *269*, 59. (b) Inushima, T.; Higashiwaki, M.; Matsui, T. *Phys. Rev. B.* **2003**, *68*, 235204. (c) Pu, X. D.; Chen, J.; Shen, W. Z.; Ogawa, H.; Guo, Q. X. *J. Appl. Phys.* **2005**, *98*, 033527. (d) Naik, V. M.; Naik, R.; Haddad, D. B.; Thakur, J. S.; Auner, G. W.; Lu, H.; Schaff, W. J. *Appl. Phys. Lett.* **2005**, *86*, 201913. (e) Dixit, A.; Sudakar, C.; Naik, R.; Lawes, G.; Thakur, J. S.; McCullen, E. F.; Auner, G. W.; Naik, V. M. *Appl. Phys. Lett.* **2008**, *93*, 142103.

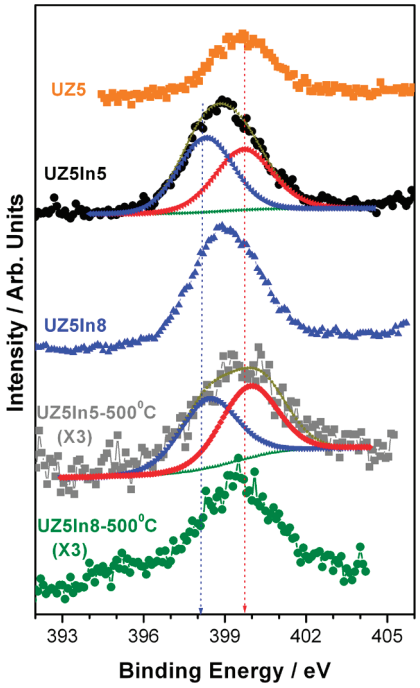

Figure 9. XPS spectra from N 1s core level of UZ5, UZ5In5, UZ5In5-500 °C, UZ5In8, and UZ5Ins8-500 °C. UZ5In5 and UZ5In5-500 °C results were deconvoluted to demonstrate the presence of nitride at 398 eV, and ammonia type nitrogen at 399.7 eV.

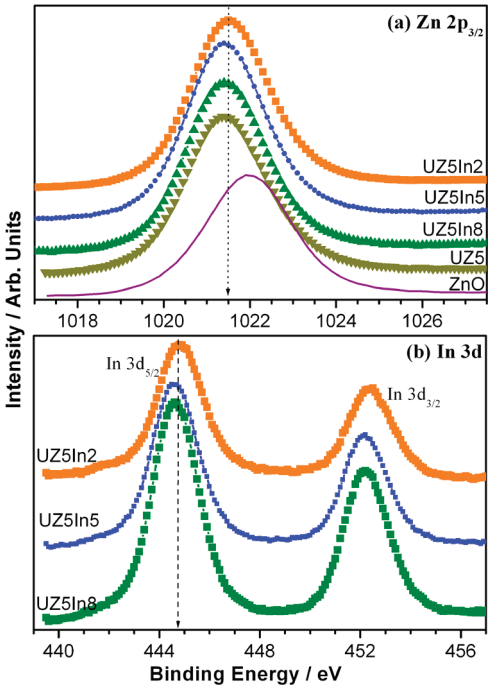

Figure 10. XPS spectra from (a) Zn $2p_{3/2}$ and (b) In 3d core levels of UZ5In2, UZ5In5, UZ5In8, ZnO, and UZ5.

leads to an exclusive solid solution of InN in ZnO. This observation is in agreement with XRD results. The lowering of the intensity of ZnO phonon modes with a concomitant increase in In-content in $(Zn_{1-z}In_z)$-$(O_{1-x}N_x)$ indicates a breaking of the total symmetry of the ZnO molecular structure. Especially, the FWHM value of E_2(high) at 436 cm^{-1} is found to be ~18 cm^{-1} for $(Zn_{1-z}In_z)(O_{1-x}N_x)$ compared to 11 cm^{-1} for ZnO. This indicates the presence of nanosized InN clusters in the samples synthesized by SCM.

Raman spectra recorded after calcination of UZ5In5 at 500 and 800 °C is shown in Figure 8b. The E_2(high) phonon modes of ZnO and InN components at 436 and 490 cm^{-1} exhibit a shift toward lower frequency after calcinations and a simultaneous decrease in FWHM. In addition, InN phonon modes (E_2(high) and A_1(LO)) intensity decreased dramatically with increasing calcination temperature supporting the disappearance of InN. Nevertheless, no In_2O_3 phonon modes have been observed on calcined materials, and this is yet to be understood.

3.6. Photoelectron Spectroscopy. XPS measurements has been performed mainly to examine the electronic structure details such as VB and oxidation states of constituent elements of $(Zn_{1-z}In_z)(O_{1-x}N_x)$ materials. Figure 9 displays the XPS results obtained from N 1s core level of UZ5, UZ5In5, UZ5In5-500 °C, UZ5In8, and UZ5Ins8-500 °C. Deconvolution has been carried out to show the overlapping nitrogen components. On $ZnO_{1-x}N_x$ materials, the N 1s core level appears to be a sharp and symmetrical peak at a BE value 399.7 eV (FWHM = 2.4 eV), indicating that the charge density on nitrogen is similar to that of ammonia type nitrogen.[4,25] However, a broad N 1s peak (FWHM = 3.1 eV) appears around 398.8 eV for $(Zn_{1-z}In_z)(O_{1-x}N_x)$ materials suggesting that there is more than one nitrogen component. Deconvolution of the N 1s core level reveals two components, and the feature at 399.7 eV is similar to the peak observed from $ZnO_{1-x}N_x$ materials. In addition, a low BE component appears at 398.1 eV. The peak at 398.1 eV could be attributed to nitrides as in GaN/InN (397.1 eV).[25] Indeed, the BE observed for nitride is somewhat higher than the typical nitrides and attributed to the influence of the surrounding majority oxide (ZnO) environment in $(Zn_{1-z}In_z)(O_{1-x}N_x)$, which is likely to make it somewhat electron deficient. Elemental mapping also exhibits a uniform distribution of nitrogen in the ZnO environment, which is likely to influence to some extent. However more detailed studies are necessary. UZ5In8 also shows similar feature as that of UZ5In5. Generally, In doping enhanced the nitrogen content very significantly, which is evident from XPS as well as EDX results.

UZ5In5 and UZ5In8 were subjected to XPS after calcination at 500 °C for 6 h. Although the above calcined materials acquired deep yellow brown color (Figure 7b inset), the surface nitrogen content apparently has decreased. It is to be noted that the peak intensity has been multiplied 3 times to show the features with clarity. However, the features observed are similar to that of as-prepared materials at the same BE, but with lower intensity. This result combined with TG/DTA results confirms that indeed $(Zn_{1-z}In_z)(O_{1-x}N_x)$ material undergoes oxidation, especially InN transforms to In_2O_3.

(25) (a) http://srdata.nist.gov/xps/ (accessed July 2009).(b) N 1s spectra were recorded with Al Kα, to ensure that no contribution from the Zn−$L_3M_{23}M_{23}$ Auger level (395−430 eV with Mg Kα) to the N 1s region. (c) Reyes-Gil, K. R.; Reyes-García, E. A.; Raftery, D. *J. Phys. Chem. C* **2007**, *111*, 14579.

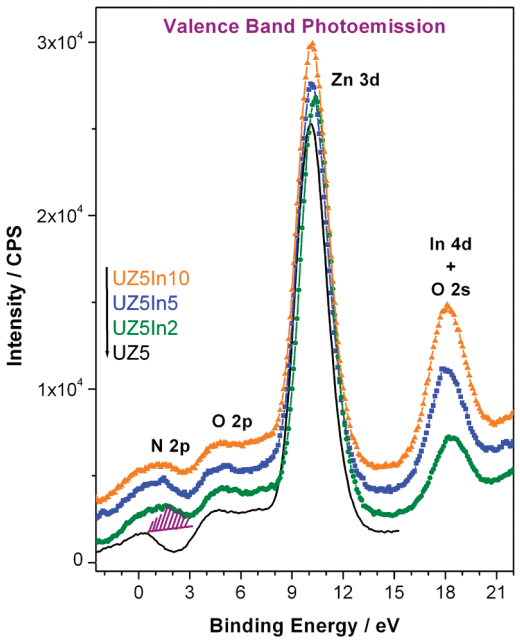

Figure 11. Valence band photoelectron spectra measured from UZ5 and $(Zn_{1-z}In_z)(O_{1-x}N_x)$ materials. The band observed at $E_F = 0$ eV is due to satellite contribution of Zn 3d level from secondary X-ray radiation. The feature observed around 2 eV is attributed to nitride 2p features.

Figure 10a shows XPS spectra of Zn $2p_{3/2}$ core level BE appearing at around 1021.5 eV for $ZnO_{1-x}N_x$, and $(Zn_{1-z}In_z)(O_{1-x}N_x)$ materials with different In-content. The above BE is significantly lower than that of ZnO (1022.0 eV).[26] Although the formal oxidation state of Zn to be +2 in all of the above materials,[25a] the electron density is relatively high on $ZnO_{1-x}N_x$ and $(Zn_{1-z}In_z)(O_{1-x}N_x)$ materials compared to ZnO. This is mainly attributed to the significant amount of nitrogen in the above materials, especially as nitride, which is electron rich and likely to influence the charge density of the neighboring cations. Likely there is some redistribution of electron density, at least locally on the above materials.

XPS data of In 3d core levels shows spin−orbit doublets at 444.7 ± 0.1 eV ($3d_{5/2}$) and 452.2 ± 0.1 eV ($3d_{3/2}$) with an energy separation of 7.5 eV (Figure 10b). BE values around 444.8 ± 0.5 eV for $3d_{5/2}$ core level has been reported for InN as well as In_2O_3 by several groups.[25a] Apparently, the BE of In 3d levels are not sensitive to chemical environment and difficult to ascertain the nature of In only from BE values. Nevertheless, it can be concluded that indium exists in the +3 oxidation state. Further, InN exhibits higher FWHM (2.1 eV), compared to In_2O_3 (1.5 eV),[27] and Figure 10b shows a FWHM of 2.2 eV supporting the nature of In to be 3+ as in InN.

VB photoelectron spectra of UZ5 and $(Zn_{1-z}In_z)(O_{1-x}N_x)$ materials has been measured with an Al Kα X-ray source and shown in Figure 11. Prominent Zn 3d and O 2p VB features were observed for all the above materials around 10 and 3−7 eV, respectively. For UZ5 (or $ZnO_{1-x}N_x$) materials, there is a band observed at Fermi level, $E_F = 0$ eV, is from satellite contribution of Zn 3d due to secondary X-ray radiations associated with Al Kα at energies higher by 9.8 (Al $K\alpha_3$) and 11.8 eV (Al $K\alpha_4$) than the parent radiation component.[28] Nonetheless, for all $(Zn_{1-z}In_z)(O_{1-x}N_x)$ materials, a new and distinct VB band feature was observed between 1 and 3 eV, in addition to the above satellite contribution. It demonstrates the intrinsic nature of this feature to $(Zn_{1-z}In_z)(O_{1-x}N_x)$ materials. Indeed the above new band (hatched area in Figure 11) is attributed to the N 2p contribution, especially from nitride. The lower BE for the nitride feature observed at the N 1s core level also supports the above conclusion. A rigid shift of VB by 0.5 eV was observed earlier by Nambu et al.[29] for N-doped TiO_2 due to N-induced features, compared to pure TiO_2. The new VB feature underscores the major change in electronic structure of the $(Zn_{1-z}In_z)(O_{1-x}N_x)$ materials due to nitride formation compared to $ZnO_{1-x}N_x$.[4] Further, this also demonstrates the change in the nature of the top of the VB from O 2p dominated on $ZnO_{1-x}N_x$ to nitride dominated on $(Zn_{1-z}In_z)(O_{1-x}N_x)$ materials. It is expected that this would significantly influence various properties, including optical and catalytic properties. In 4d and O 2s shallow core levels appear around 18 eV, indicating the overlap in their energy. However, the In 4d level is far away from the VB and unlikely to influence the VB energy due to the N/O 2p−In 4d (p−d) repulsion, as suggested earlier. Likely, N 2p states from VB and 4p/5p states from CB could have an attractive interaction and probably a reason for the band gap reduction mechanism. More detailed studies are required to confirm the above point.

3.7. SIMS Analysis. Secondary-ion mass spectrometry (SIMS) was employed to explore the nature of different zinc and nitrogen related species in the as-prepared $(Zn_{1-z}In_z)(O_{1-x}N_x)$ materials, especially the homogeneity of doping from surface to bulk. Representative SIMS results are shown in Figure 12. Species that exhibited < 20 counts/s were not considered due to high noise level. An initially recorded mass spectrum with significant intensity demonstrated the presence of different species, namely, Zn, In, ZnO, ZnN, InN, InO, ZnNIn, N, and O. Secondary-ion intensities of the relevant species are shown in Figure 12, as a function of sputtering time or depth for (a) UZ5, (b) UZ5In5, and (c) UZ5In10. No significant decrease in counts/intensity of any species was observed with sputtering time emphasizes the bulk doping in ZnO, and the uniformity of the substitution throughout

(26) (a) Velu, S.; Suzuki, K.; Vijayaraj, M.; Barman, S.; Gopinath, C. S. *Appl. Catal., B* **2005**, *55*, 287. (b) Anand, R.; Hegde, S. G.; Rao, B. S.; Gopinath, C. S. *Catal. Lett.* **2002**, *84*, 265.
(27) Lee, I. J.; Yu, C.; Shin, H.-J.; Kim, J.-Y.; Lee, Y. P.; Hur, T.-B.; Kim, H.-K. *Thin Solid Films* **2007**, *515*, 4691.
(28) (a) Wagner, C. D.; Riggs, W. M.; Davis, L. E.; Moulder, J. F.; Muilenberg, G. E. *Handbook of X-ray photoelectron spectroscopy*; Perkin-Elmer Corporation: Eden Prairie, MN, 1979. (b) Gopinath, C. S.; Subramanian, S.; Huth, M.; Adrian, H. *J. Electron Spectrosc. Relat. Phenom.* **1994**, *70*, 61. (c) Gopinath, C. S.; Subramanian, S.; Sumana Prabhu, P.; Ramachandra Rao, M. S.; Subba Rao, G. V. *Physica C* **1993**, *218*, 117.
(29) Nambu, A.; Graciani, J.; Rodriguez, J. A.; Wu, Q.; Fujita, E.; Fdez Sanz, J. *J. Chem. Phys.* **2006**, *125*, 094706.

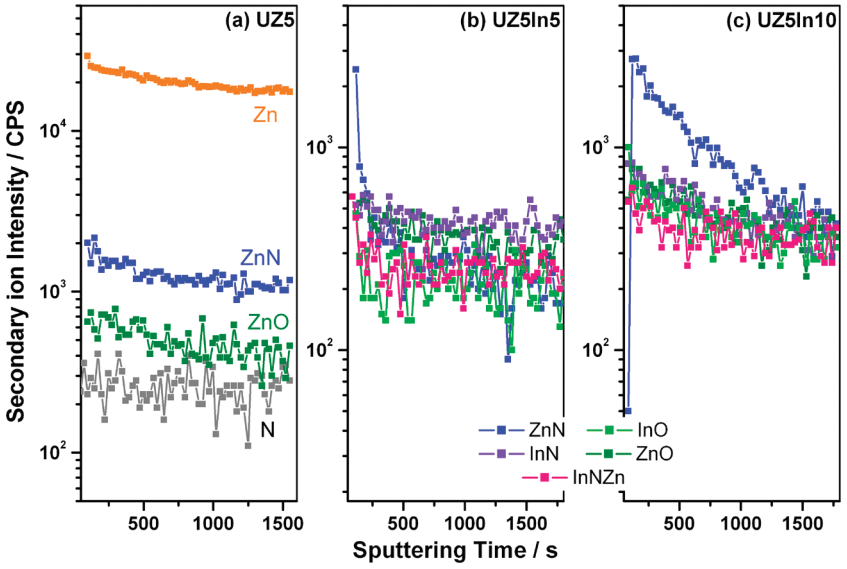

Figure 12. SIMS measurements displaying secondary ion intensities measured as a function of sputtering depth or time obtained from (a) UZ5, (b) UZ5In5, and (c) UZ5In10.

the bulk. The higher count rates observed for the ZnN fragment than the ZnO fragment, despite ZnO being the host lattice in UZ5 (Figure 12a), are attributed to the different ionization capacity of emitted species, and this is strongly dependent on the local surface characteristics of the materials, known as the matrix effect.[30] Indeed, comparable count rates observed for the five species given in Figure 12b and c underscore the idea that the materials surface chemistry is not dependent on the bulk composition.

Direct observation of ZnNIn and InN fragments from UZ5In5 and UZ5In10 underscores the existence of a solid solution of InN in ZnO. Indeed, the ZnNIn fragment suggests a direct interaction between N^{3-} to In as well as Zn. The fact that signal intensities remain constant at deeper levels from the surface highlights the uniform distribution throughout the material. This conclusion corroborates well with Raman and XPS results. InO and ZnNIn species are observed with comparable count rates for 5 and 10% In containing materials, suggesting the nature of InN clusters to be in the nanosized regime. This might be true since no separate features for InN are observed in XRD, even up to In = 10%, rather than a shift to lower angle and a broadening of all features observed. The fact that no nitric oxide (NO) related species was observed suggests the efficacy of the combustion method to introduce N^{3-} into the ZnO lattice in an overall reductive atmosphere.[4,6]

The presence of InN in $(Zn_{1-z}In_z)(O_{1-x}N_x)$ supported by physicochemical analysis underscores the importance of the reaction atmosphere generated in the present experimental conditions. It is also to be noted that typical nitridation of oxides requires passing ammonia for several hours to a couple of days at high temperatures.[31] Nonetheless, the formation of a solid solution of InN in ZnO hints at the in situ generation of high flux NH_3 at high temperatures (~700 °C) under the present preparation conditions. Indeed gas-phase analysis of evolved gases shows predominantly NH_3 along with some CO_2. However, a uniform distribution of small clusters of InN in ZnO is unexpected, especially under the vigorous reaction conditions employed in the present work. Theoretical calculations on GaN by Schaefer et al.[32] predict a small clusters of a size between 30 and 40 oligomers of GaN under similar pyrolysis conditions and is in good agreement with our experimental results. We suggest that the SCM may be adopted to prepare such solid solutions in a short period of time, which are otherwise difficult to prepare.

3.8. Acceptor (and Solvent) Free Catalytic Dehydrogenation of 2-Butanol. Dehydrogenation of alcohols to carbonyl (aldehyde or ketone) compounds is an important transformation in synthetic organic chemistry. Lately, much attention has been paid to the development of different catalysts for the highly efficient oxidation of alcohols using O_2 or air as the oxidant because of the necessity of replacing stoichiometric reactions.[33] Although it is better than using stronger and more hazardous oxidizing agents, it would be unique to carry out a dehydrogenation reaction without any acceptor, such as oxygen.[34] This is important as it (a) eliminates the formation of water, a byproduct which often deactivates catalysts and necessitates difficult purification of products, and (b) suppresses overoxidation of the products (aldehyde or ketone) to acids and/or CO_2, and additionally, it produces

(30) Chakraborty, P. *Ion beam analysis of surfaces and interfaces in condensed matter systems*; Chakraborty, P., Ed.; Nova Science Publishers: New York, 2002.
(31) Maeda, K.; Teramura, K.; Lu, D.; Takata, T.; Saito, N.; Inoue, Y.; Domen, K. *Nature* **2006**, *440*, 295.
(32) Timoshkin, A. Y.; Schaefer, H. F., III J. Phys. Chem. A **2008**, *112*, 13180 and references therein.
(33) (a) Mallat, T.; Baiker, A. *Chem. Rev.* **2004**, *104*, 3037. (b) Anderson, R. A.; Griffin, K.; Johnson, P.; Alsteres, P. L. *Adv. Synth. Catal.* **2003**, *345*, 517. (c) Sheldon, R. A. *Green Chem.* **2000**, *2*, G1.
(34) (a) Kim, W.-H.; Park, I. S.; Park, J. *Org. Lett.* **2006**, *8*, 2543. (b) Mitsudome, T.; Mikami, Y.; Funai, H.; Mizugaki, T.; Jitsukawa, K.; Kaneda, K. *Angew. Chem. Inter. Ed.* **2008**, *120*, 144.

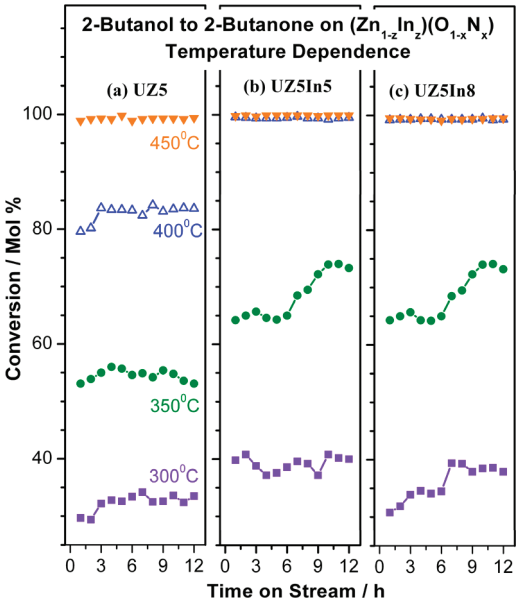

Figure 13. Catalytic conversion of 2-butanol on (a) UZ5, (b) UZ5In5, and (c) UZ5In8 materials in the temperature range between 300 and 450 °C.

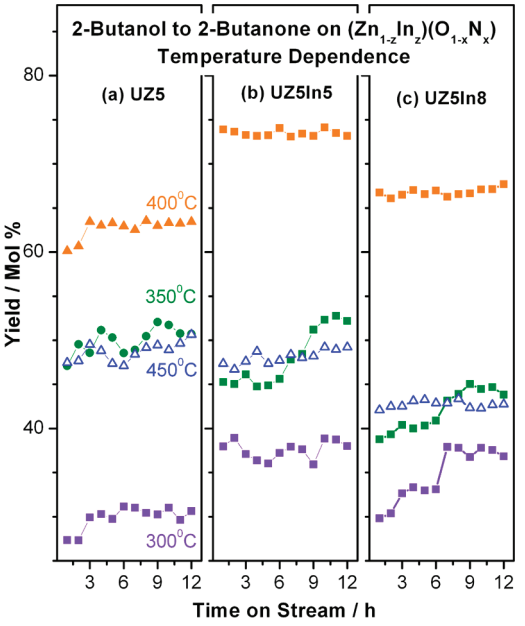

Figure 14. Methyl ethyl ketone (MEK) yield obtained on (a) UZ5, (b) UZ5In5, and (c) UZ5In8 in the temperature range between 300 and 450 °C.

H_2, which is a feedstock for energy generation. Indeed there are few recent reports available on the above acceptor free catalytic dehydrogenation of alcohols using hydrotalcite or oxyhydroxide as the catalytic support.[32] Nonetheless, these methods employ noble metal as the active catalyst component on the above support materials and uses either toluene or xylene as the solvent, with a typical ratio of 1 mmol of alcohol in 5 mL of solvent, for a reaction period of several hours (up to 40 h) at temperatures between 80 and 150 °C.[34] Further gas-phase dehydrogenation of alcohols through heterogeneous catalysis has definite advantages over other methods, and it is necessary to develop catalytic dehydrogenation for industrial applications.

ZnO being a traditional catalyst employed for dehydration and dehydrogenation reactions,[35] $(Zn_{1-z}In_z)(O_{1-x}N_x)$ materials also explored for catalytic dehydrogenation of 2-butanol to methyl ethyl ketone (MEK) without any noble metal and by vapor phase heterogeneous catalysis. MEK is a good solvent, especially for coating applications and also used in dry erase markers as the solvent for the erasable dye. Figure 13 shows the catalytic conversion of 2-butanol as a function of time on stream (TOS) for three different catalyst compositions (UZ5, UZ5In5, and UZ5In8) between 300 and 450 °C. MEK formed as a major product along with some gaseous products, like CO_2 and butene. There is hardly any catalytic activity observed below 300 °C for this particular reaction. Initially, the reaction was carried out at different space velocity values and observed that weight hourly space velocity (WHSV) = 5 gave maximum conversion, and hence, all our studies have been carried out at this value. Catalytic conversion of 2-butanol increases steadily, with increasing temperature, from 300 °C (Figure 13). An important observation to be noted is that catalytic conversion remains at the same level from the beginning for 12 h for all catalyst compositions. 30−40% catalytic conversion was observed at 300 °C for all catalyst composition increases to 100% conversion at 450 °C for UZ5, but at 400 °C for In-containing materials. The 100% conversion obtained with UZ5In5 at 400 °C suggested the influence of InN content toward better activity. However, with further increase in In-content, the catalyst (UZ5In8 and UZ5In10) does not show increase in overall activity hinting that optimum activity is with UZ5In5. Nonetheless, pure ZnO exhibits significant conversion from 400 °C and above,[35b] indicating that the introduction of N in ZnO (UZ5) definitely increased the activity at relatively lower temperatures.

Figure 14 displays the MEK yield observed for all three catalyst compositions between 300 and 450 °C as a function of TOS. At 300 °C, MEK yield is observed between 30 and 40 mol % irrespective of the catalyst compositions. However with increase in temperature (up to 400 °C) the MEK yield increases up to 64% on UZ5, and then, it decreases to 50% at 450 °C. A similar trend was observed with In-containing catalysts also. However, the highest yield around 75% was observed with UZ5In5 at 400 °C. The selectivity and yield of MEK decreases for all the catalysts above 400 °C. There is significant secondary gaseous product, butene, which occurs due to the dehydration reaction and could be minimized by lowering the temperature, especially between 350 and 400 °C; further studies are necessary to optimize the conditions. It is to be noted that introduction of In induces Lewis acidity and is likely responsible for higher catalytic activity, and it is well-known that acid−base properties

(35) (a) Lazier, W. A.; Adkins, H. *J. Am. Chem. Soc.* **1925**, *47*, 1719. (b) Ravi, S.; Raghunathan, T. S. *Ind. Eng. Chem. Res.* **1988**, *27*, 2050. (c) Raizada, V. K.; Tripathi, V. S.; Lal, D.; Singh, G. S.; Dwivedi, C. D.; Sen, A. K. *J. Chem. Technol. Biotechnol.* **1993**, *56*, 265.

change the catalytic activity.[36] An important point to be noted is the stable conversion and yield for all the three catalysts over the entire reaction period (12 h). No decline in activity indicates no or very little change in the nature of the material surface characteristics. All the above studies which have been carried out in a static air or nitrogen atmosphere exhibit same activity demonstrating that no acceptor molecules are required. Further studies are in progress.

4. Conclusion

$(Zn_{1-z}In_z)(O_{1-x}N_x)$ materials were prepared by simple solution combustion method and characterized by a variety of physicochemical, structural, spectroscopy, microscopy, and catalytic measurements for the dehydrogenation reaction. The above detailed studies suggest the nature of the $(Zn_{1-z}In_z)(O_{1-x}N_x)$ material to be a solid solution of InN in ZnO. Except for a minor lattice expansion, no significant change in the hexagonal wurtzite structure was observed even up to 10% InN in $(Zn_{1-z}In_z)(O_{1-x}N_x)$ materials. Even though combustion method involves high temperatures up to 1000 °C, almost homogeneous nanosized (200−300 nm) particles were observed by SEM. Elemental mapping of $(Zn_{1-z}In_z)$-$(O_{1-x}N_x)$ materials displays a homogeneous distribution of doped elements and InN formation. Good thermal stability, at least up to 500 °C, was identified from thermal analysis and supported by other characterization methods.

A new absorption band in the visible region was observed with the onset of absorption around 550 nm. UV−visible absorption and valence band XPS studies demonstrate the creation of a new band derived from N 2p states of nitride just above the O 2p VB, primarily responsible for the reduction of optical band gap to 2.3 eV for $(Zn_{1-z}In_z)(O_{1-x}N_x)$. Raman spectral studies directly show the linkage between Zn/In and N, and E_2(high) and A_1(LO) modes corresponding to InN were observed clearly. XPS data indicates that there are two types of nitrogen on $(Zn_{1-z}In_z)(O_{1-x}N_x)$ with different charge density; the N 1s BE that appears at 398 eV (399.7 eV) corresponds to nitride (ammonia). All the above studies and characterizations demonstrate that $(Zn_{1-z}In_z)$-$(O_{1-x}N_x)$ is indeed a solid solution of InN in ZnO. Although the solid solution indicates the complete disordering of cations and anions to corresponding lattice positions, the present set of results obtained from several methods indicate the presence of very small nanoclusters of InN in the above solid solution, which is likely to stabilize the $(Zn_{1-z}In_z)(O_{1-x}N_x)$ material as well as to improve the nitrogen content. More work is needed to confirm the above aspect.

$(Zn_{1-z}In_z)(O_{1-x}N_x)$ materials also show high conversion and yield toward methyl ethyl ketone from catalytic dehydrogenation of 2-butanol and without any acceptors. The present study demonstrates the multifunctional nature of $(Zn_{1-z}In_z)(O_{1-x}N_x)$ materials, and it is worth exploring further for applications such as optoelectronics and photocatalysis after suitable modifications.

Acknowledgment. This work is dedicated to Prof. P.T. Manoharan, IIT, Madras, on the occasion of his 75th birthday. M.M., K.S., and B.S. thank CSIR, New Delhi, for research fellowship.

Supporting Information Available: SI-1 for EPR measurements and SI-2 for particle size distribution by dynamic light scattering of $(Zn_{1-z}In_z)(O_{1-x}N_x)$ materials. This material is available free of charge via the Internet at http://pubs.acs.org.

(36) (a) Mathew, T.; Tope, B. B.; Shiju, N. R.; Hegde, S. G.; Rao, B. S.; Gopinath, C. S. *Phys. Chem. Chem. Phys.* **2002**, *4*, 4260. (b) Mathew, T.; Shylesh, S.; Devassy, B. M.; Satyanarayana, C. V. V.; Rao, B. S.; Gopinath, C. S. *Appl. Catal., A* **2004**, *273*, 35. (c) Waghmode, S. B.; Vetrivel, R.; Hegde, S. G.; Gopinath, C. S.; Sivasanker, S. *J. Phys. Chem. B* **2003**, *107*, 8517.